Nanomed Res J 8(1): 69-88, Winter 2023

RESEARCH ARTICLE

Curcumin derivative loaded albumin nanoparticles: preparation, molecular interaction study and evaluation of physicochemical properties, in-vitro release and cytotoxicity

Masoumeh Keshavarz[1], Maryam Saeidifar[1], Navid Ahmadi Nasab[2,3], Omid Safa[4], Sara Nikoofal- Sahlabadi[5,*]

[1]Department of Nanotechnology and Advanced Materials, Materials and Energy Research Center, Karaj, Iran

[2]Hormoz Research Center, University of Hormozgan, Bandar Abbas, Iran

[3]Department of Marine Biology, Faculty of Marine Science and Technology, University of Hormozgan, Bandar Abbas, Iran

[4]Department of Clinical Pharmacy, Faculty of Pharmacy, Hormozgan University of Medical Sciences, Bandar Abbas, Iran

[5]Department of Pharmaceutics, Faculty of Pharmacy, Hormozgan University of Medical Sciences, Bandar Abbas, Iran

ARTICLE INFO

Article History:
Received 11 Oct 2022
Accepted 08 Nov 2022
Published 15 Feb 2023

Keywords:
Desolvation
Synthesis
Nanomedicine
Controlled Release
Kinetics, Cancer

ABSTRACT

Albumin nanoparticles have shown great potential in cancer drug delivery. In this study, firstly, fluorescence spectroscopy and molecular docking studies indicated a predominant hydrophobic interaction between 2,6-bis(3,4-methylenedioxybenzylidene)-1-cyclohexanone (BMC) derivative of curcumin and bovine serum albumin (BSA). Then, BMC was loaded in BSA nanoparticles (BSANPs) via adsorption and entrapment approaches based on desolvation technique. The structural changes and loading of BMC in BSANPs were confirmed using UV-Vis, FTIR and TGA analysis. The effect of loading process on physicochemical properties was evaluated by DLS, FESEM and calculating of the drug loading (DL) and entrapment efficiency (EE) percentages. Formulations prepared through entrapment method (BMC@BSANPs-E) showed smaller particle sizes than adsorption (BMC@BSANPs-A). However, mean particle size of NPs were controlled between 159.2±3.45 to 201.7±1.57 nm. Also, acceptable negative values were achieved for zeta potential and formulations showed spherical morphology. Larger DL% were obtained for BMC@BSANPs-A, however, higher EE% were observed for BMC@BSANPs-E. While both formulations showed a sustained release behavior in-vitro with more release in acidic pH than neutral conditions, greater cumulative release percentage was obtained for BMC@BSANPs-A. BMC release in both formulations followed the first order kinetic model and release mechanism was controlled by Fickian diffusion. Finally, cytotoxicity tests on MCF-7 cancer cells showed the improvement of the anti-cancer effect of the formulations in comparison with the free BMC.

How to cite this article
Keshavarz M., Saeidifar M., Ahmadi Nasab N., Safa O., Nikoofal- Sahlabadi S., Curcumin derivative loaded albumin nanoparticles: preparation, molecular interaction study and evaluation of physicochemical properties, in-vitro release and cytotoxicity. Nanomed Res J, 2023; 8(1): 69-88. DOI: 10.22034/nmrj.2023.01.007

INTRODUCTION

In recent decades, cancer has become one of the most challenging global threats to human health and life. Among the leading strategies to overcome this disease, nanomedicine has opened promising horizons in terms of using effective delivery systems for promoting the efficacy and reducing the side effects of cancer diagnostic and therapeutic agents (1). The nanocarriers used in this field include different categories, among which albumin NPs have attracted prominent attention due to desirable characteristics, such as endogenous nature, biocompatibility and biodegradability, non-immunogenicity, non-toxicity, chemical stability and high aqueous solubility (2-5). Being the most abundant protein in the plasma with

* Corresponding Author Email: *nikoofalsara@gmail.com*

a long circulating half-life, albumin possesses different binding sites for both hydrophilic and hydrophobic compounds. The presence of amine, thiol and carboxylic acid functional groups confers the possibility of both covalent bonding and non-covalent interaction between this biological macromolecule and a variety of therapeutic agents (6). Accordingly, albumin NPs are able to transport pharmaceutical compounds, especially hydrophobic drugs in the physiological environment, and improve pharmacokinetic and biodistribution of their payloads through conserving them from rapid metabolism and elimination (7, 8). In addition, nanometer dimensions allow albumin NPs to target the tumor sites in a passive manner via the enhanced permeability and retention (EPR) mechanism. Furthermore, active targeting through gp60 receptors and SPARC pathway, both overexpressed in tumor cells, promote accumulation of anti-cancer agents in tumor sites (9, 10).

Various methods including emulsification, desolvation, thermal gelation, self-assembly, nano-spray drying and microfluidic mixing are used for preparation of albumin NPs. Amongst these techniques, desolvation is one of the common ones, widely used due to ease of process and reproducibility (7, 11). In this method, dropwise addition of a desolvating agent like ethanol or acetone to the albumin aqueous solution under stirring conditions, leads to the change in tertiary structure of protein due to disruption of the electrostatic and hydrophobic interaction's balance. As the result, the water solubility of albumin decreases, it undergoes phase separation and the precipitate of NPs are formed (6, 12). Moreover, a crosslinker agent, often glutaraldehyde, is needed for stabilizing the obtained NPs. In crosslinking process, carbonyl moieties of glutaraldehyde are attacked by amine groups in lysine and arginine residues of protein which results in the formation of Schiff bases (13). In desolvation procedure, different parameters such as albumin concentration, pH, desolvating agent to albumin solution ratio, rate of desolvating agent addition, stirring rate, type and ratio of the crosslinker, need to be carefully controlled because of their significant role on the NPs size. Indeed, the size of NPs not only is involved in the loading amount of the drug, but also affect cellular uptake of NPs (14, 15).

1,7-bis-(4-hydroxy-3-methoxyphenyl)-1,6-heptadiene-3,5-dione or curcumin is a natural hydrophobic polyphenol extracted from the rhizome of a plant named *curcuma longa*. Besides pleiotropic features such as anti-inflammatory, antioxidant, antimicrobial and wound healing activities, curcumin has been illustrated to be effective in inhibition of tumor cells growth and proliferation in numerous studies. Despite the unique properties of curcumin, very low water solubility and bioavailability as well as physiological instability has limited its clinical applications (16-20). Curcumin is a symmetric molecule with a β-diketone skeleton and two aromatic groups (Fig. 1). *In-vivo* and *in-vitro* studies have shown that the presence of methylene active group and β-diketone moiety are involved in physiological instability and rapid metabolism of curcumin. On the other hand, efficacy of cyclohexanone derivatives of curcumin to increase cytotoxicity against estrogen receptor negative cancer cells has been reported (21, 22). Also, the hydroxyl groups of curcumin are altered in kidneys, liver, and intestinal mucosa, produce the curcumin glucuronide and curcumin sulfate, which have low bioactivity and efforts have been made to replace these groups as well (23, 24). 2,6-bis(3,4-methylenedioxybenzylidene)-1-cyclohexanone (BMC) is a cyclohexanone derivative of curcumin in which the methylenedioxy groups has replaced the hydroxyl groups (Fig. 1). According to the research carried out by Ramshini et al., this compound showed more stability and bioavailability than curcumin with an improved cytotoxicity against MCF-7 cancer cell line (25).

In the present study, the interaction of BMC with bovine serum albumin (BSA) was investigated for the first time with fluorescence spectroscopy and molecular docking techniques. Subsequently, BSA nanoparticles were used as a carrier for BMC hydrophobic compound for improving its solubility and anticancer properties. Two desolvation based procedures, adsorption and entrapment, were used to prepare BMC loaded BSANPs. Then, physicochemical properties of the two prepared formulations were compared and drug release behavior as well as kinetic of release were evaluated by mathematical models. Eventually, cytotoxic effects of the formulations *in-vitro* was investigated against MCF-7 cancer cell line.

MATERIALS AND METHODS

Materials

Bovine serum albumin (BSA > 99% w/w), 2,6-bis(3,4-methylenedioxybenzylidene)1-cyclohexanone (BMC > 99% w/w), glutaraldehyde (25% w/w solution in water), phosphate buffer saline tablet (PBS), dialysis tube (molecular weight cut off of 12 kDa), RPMI-1640 culture medium, MTT

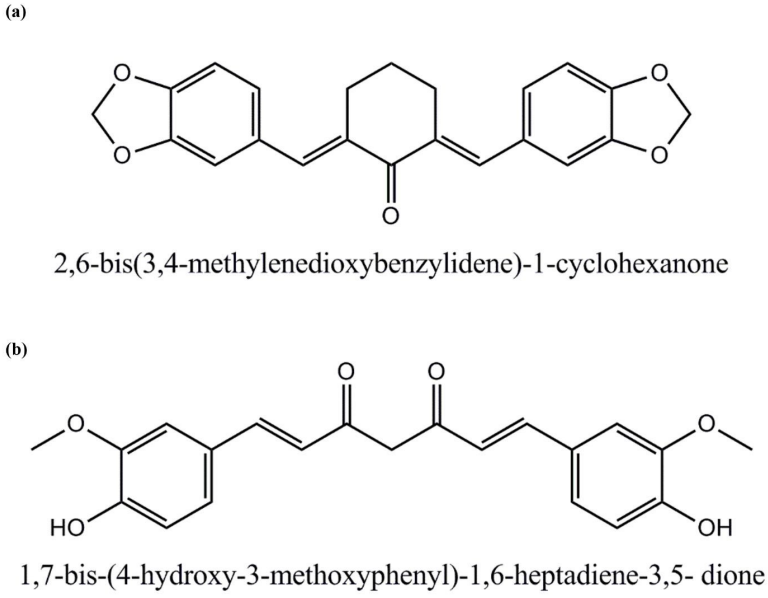

Fig. 1. 2D-ChemDraw structures of (a) 2,6-bis(3,4-methylenedioxybenzylidene)1-cyclohexanone (BMC), (b) 1,7-bis-(4-hydroxy-3-methoxyphenyl)-1,6-heptadiene-3,5- dione (curcumin)

powder (3-[4,5-dimethylthiazol-2-yl]-2,5-diphenyl tetrazolium bromide), penicillin and streptomycin antibiotics and trypsin-EDTA solution (0.25% w/v) were purchased from Sigma-Aldrich (St. Louis, Missouri, United States). Fetal bovine serum (FBS) was prepared from Gibco (Waltham, Massachusetts, United States). Hydrochloric acid (37% w/w) and ethanol was purchased from Merck (Germany). All other reagents and solvents were analytical or HPLC grade. Ultra-pure deionized water was used for preparing all solutions.

Fluorescence spectroscopy studies

Fluorescence measurements for investigating the interaction of BMC compound and BSA protein were performed using a Cary eclipse fluorescence spectrophotometer. For this analysis, the excitation wavelength was set on 280 nm and the BSA emission spectra with a fixed concentration of 1.5 µM was obtained in the range of 300-500 nm in the absence and presence of the BMC at different concentrations of 0.5, 1, 1.5, 2, 2.5, 3, 4, 5, 7.5 and 10 µM. The excitation and emission slit widths both were adjusted on 5 nm and measurements were carried out at two temperatures of 298 and 310 K using a fluorescence cuvette with 1 cm path length.

The quenching mechanism was determined by applying the Stern-Volmer equation to fluorescence data as follow (26):

$F_0/F=1+kq\ \tau_0\ [Q]=1+K_{SV}\ [Q]$ Equation (1)

Where, F_0 and F are the fluorescence intensity in the absence and presence of BMC, respectively, k_q is the biomolecular quenching rate constant, τ_0 is the life time of the fluorophore in the absence of BMC as quencher and is 10^{-8} s for BSA, [Q] is the BMC concentration and K_{SV} is the Stern–Volmer quenching constant.

Also, the binding parameters were determined using following equation:

$\log \Delta F/F = \log K_b+n\log[Q]$ Equation (2)

Where ΔF is the difference between F_0 and F, K_b is the binding constant and n is the number of binding sites (27).

Finally, the thermodynamic parameters, including Gibbs free energy (ΔG°), enthalpy (ΔH°) and entropy (ΔS°) changes were calculated from Van't Hoff equation (28):

$\ln K_b=(-\Delta H°)/RT+(\Delta S°)/R$ Equation (3)

$\Delta G°=-RT \ln K_b=\Delta H°-T\Delta S°$ Equation (4)

R and T are the ideal gas constant (8.314 J/mol.K) and absolute temperature, respectively.

Molecular docking

Molecular docking studies were performed using AutoDockTools version 1.5.7. BMC molecule was designed by ChemBio3D Pro 12.0 and geometry was optimized using MM2 force field method with the minimum RMS of 0.001. The crystal structure of BSA with PDB code of 3V03 was prepared from RCSB Protein Data Bank. BSA was considered as

rigid molecule and BMC as a flexible one on BSA. Hydrogen atoms were added and non-functional water molecules were removed. Kollman and Gasteiger partial charges were also assigned to the protein and ligand. For global optimum binding position search, the Lamarckian genetic algorithm technique was used with following parameters:

Population size: 150, maximum number of generations: 27000, maximum number of energy evaluations: 2.5×10^6, mutation rate: 0.02 and crossover rate: 0.8.

The docking process was performed for 100 runs and the conformations were ranked according to the docked energy.

Synthesis of BSANPs and BMC loaded BSANPs

Desolvation method was used for synthesis of formulations with some modifications (11). For preparing of BMC@BSANPs-A, adsorption method, 20 mg of BSA was dissolved in 1 mL ultrapure water and stirred at 500 rpm for 20 min. Subsequently 4 mL ethanol as a desolvating agent was added dropwise to BSA solution at a rate of 1 mL/min and stirred for more 10 min. Then, 12 µL of 8% glutaraldehyde was added as crosslinker and the solution was stirred at 500 rpm for 24 h at 25 ℃. To remove any free glutaraldehyde and ethanol, the nanoparticle colloidal dispersion was purified by centrifugation at 12,000 rpm for 10 min at 25 ℃. Centrifugation was performed in 3 cycles and at every step the NPs were dispersed in 5 mL ultrapure water using ultrasonication for 5 min. Finally, the BSANPs were dispersed in 1 mL ultrapure water and stored at 4℃ in darkness or frozen overnight at -20 and lyophilized at -55℃ for further tests. For loading of BMC on BSANPs, BMC in ratios of 1:10, 1:20 and 1:40 to BSA (w/w) was dissolved in 4 mL ethanol and added to BSANPs aqueous solution and stirred at 500 rpm for 24 h in darkness. Then the colloidal dispersion was centrifuged at 12,000 rpm for 10 min to remove the ethanol and unbonded drug.

For BMC@BSANPs-E formulation preparation, BMC was loaded during the synthesis process of BSANPs. For this purpose, BMC (1:10, 1:20 and 1:40 (w/w) to BSA) was dissolved in 4 mL ethanol and added to 20 mg/mL BSA aqueous solution in desolvation step. Similar to adsorption method, after formation of NPs, 12 µL of 8% glutaraldehyde was added for crosslinking and after 24 h stirring at 500 rpm, suspension was centrifuged 3 times at 12,000 rpm for 10 min at 25 ℃ and final NPs were dispersed and stored in water or lyophilized for further tests.

Characterization of NPs

Hydrodynamic particle size, polydispersity index (PDI) and zeta potential were determined by dynamic light scattering (DLS) technique, using a Horiba SZ-100 nanoparticle analyzer. The NPs were diluted with ultrapure water (1:100 v/v) and measurements were performed at 25 ℃ using a scattering angle of 90°. The morphology of NPs was studied using field emission scanning electron microscope (FESEM), model TESCAN MIRA 3, and transmission electron microscope (TEM) model ZEISS LEO 906 E. To prepare FESEM samples, a drop of NPs colloidal dispersion was placed on a silicon slice and dried in air. The samples were coated by gold to make them conductive. The samples were imaged at 10 kV using the secondary electrons mode. TEM samples were prepared by drying the NPs colloidal dispersion on a copper grade. Also, the UV-visible absorption spectra of Pure BSA, BSANPs, BMC, BMC@BSANPs-A and BMC@BSANPs-E at the wavelength range of 200-600 nm were determined by spectrophotometer (UNICO 2150-UV) at ambient temperature and the wavelength of maximum intensity were determined for BSA and BMC. The chemical structure of samples as well as confirmation of drug loading in NPs were investigated by FTIR spectroscopy. For this test, 1 mg of the samples were mixed with 100 mg KBr powder and pressed in the form of disks. The FTIR spectra of the samples were obtained in the range of 4000-400 cm^{-1} using a Bruker ALPHA II FTIR spectrometer. Moreover, TGA analysis was used for the examination of BMC, BSA, BMC@BSANPs-A and BMC@BSANPs-E formulations weight loss using PL-STA 1640 instrument. The analysis was performed on 5 mg of each sample, up to 600℃ in air atmosphere. The heating rate set on 10 ℃/min.

Determination drug loading and entrapment efficiency

To calculate the drug loading percentage (DL%) and entrapment efficiency percentage (EE%), the supernatant of centrifugation step, in each of the loading methods, was collected and analyzed by UV-Vis spectrophotometer. The standard curves of BSA and BMC were plotted by measuring the absorption of maximum intensity at 283 and 389 nm respectively in different concentrations (Fig S1). DL% and EE% were calculated using the

following equations:

$$DL\% = \frac{wight\ of\ BMC\ in\ NPs}{wight\ of\ BSA\ NPs + wight\ of\ BMC\ in\ NPs} \times 100$$ Equation (5)

$$EE\% = \frac{wight\ of\ BMC\ in\ NPs}{initial\ total\ wieght\ of\ BMC} \times 100$$ Equation (6)

In-vitro studies

Drug release study

Dynamic dialysis method was used to evaluate *in-vitro* release behavior of BMC from BMC@BSANPs-A and BMC@BSANPs-E formulations under two conditions with acidic and neutral pH of 5.5 and 7.2. For this purpose, 1 mL of each formulation (equivalent to 0.5 mg of drug) was poured and trapped inside a dialysis bag with 12 KDa molecular cut-off and immersed in 10 mL of PBS-ethanol release medium with a volume ratio of 6:4 v/v. HCl was added to the media to obtain an acidic pH. Drug release process was performed at 37 ℃ under shaking at 100 rpm in darkness. At predetermined intervals from 15 min to 120 h, 3 mL of each medium was withdrawn and replaced with equal amount of fresh one to maintain sink conditions. The amount of released BMC was obtained by analyzing the withdrawn samples by UV-Vis spectrophotometer at BMC characteristic peak (absorption at 389 nm) and applying the obtained equations from plotted standard curves of BMC in release media (Fig. S2). The cumulative release percentage was calculated using the below equation and the graph of release percentage was drawn versus time.

$$Cumulative\ release(\%) = \frac{amount\ of\ released\ drug\ at\ each\ time}{total\ amount\ of\ loaded\ drug} \times 100$$

Equation (7)

Drug release kinetics

The mechanism of BMC release from BSANPs was investigated using zero-order, first-order, Korsmeyer-Peppas, Higuchi and Hixon-Crowell kinetic models as follow:

$$M_t / M_\infty = k_0 t$$ Equation (8)

$$M_t / M_\infty = 1 - \exp(-k_1 t)$$ Equation (9)

$$M_t / M_\infty = k_{KP} . t^n$$ Equation (10)

$$M_t / M_\infty = k_H . t^{0.5}$$ Equation (11)

$$M_t / M_\infty = 1 - (1 - k_{HC} . t)^3$$ Equation (12)

Where M_t is the amount of BMC released at a given time t and M_∞ is the total amount of BMC loaded into the NPs. Also, k_0, k_1, k_H, k_{HC}, k_{KP} and n are constants for the zero-order, first-order, Higuchi, Hixon-Crowell and Korsmeyer-Peppas models, respectively. Nonlinear regression method was used to fit the models with the release experimental data.

Cell culture

MCF-7 human breast cancer cell line was prepared from the cell bank of Pasteur Institute (Tehran, Iran). The cells were grown in culture flasks containing RPMI 1640 media with 10% FBS and 1% Penicillin and Streptomycin (Pen-Strep) antibiotics. Then cells were placed in incubator with a humidified atmosphere by 5% CO_2 at 37℃. The culture media was replaced every 2 days.

Cytotoxicity study

The *in-vitro* cytotoxicity studies were assessed against MCF-7 cells using MTT assay according to the manufacturer's instructions. Briefly, the cells were seeded in 96 well microplate (8×10^3 cells per well) for 24 h. Then, the cells treatment was performed with 50-350 µg/mL of BSANPs or 5–60 µg/mL of free BMC and equivalent doses of BMC@BSANPs-A and BMC@BSANPs-E formulations. After incubation for 24 and 72 h, media were replaced by fresh one containing 0.25 mg/mL MTT reagent (without phenol red) and incubated for 3 h at 37°C until purple precipitate was visible. Then, each medium was carefully removed and 150 µL DMSO per well was added and incubation was done for about 15 min at 25 °C. Spectrophotometric absorbance of the formazan solution was obtained at 570 nm by Bio Tek ELx808 model microplate reader. Results were reported as percentage of cell viability and IC_{50} values. Percentage of cell viability was calculated according to equation (9) and untreated cells were considered as control samples.

% cell viability = 100 × (OD sample - OD control) / OD control. Equation (13)

Statistical analysis

SPSS 26 software was used for statistical analysis following one-way analysis of variance (ANOVA). All data were presented as the mean ± standard deviation of three independent tests. The p-value < 0.05 was considered significant in all tests.

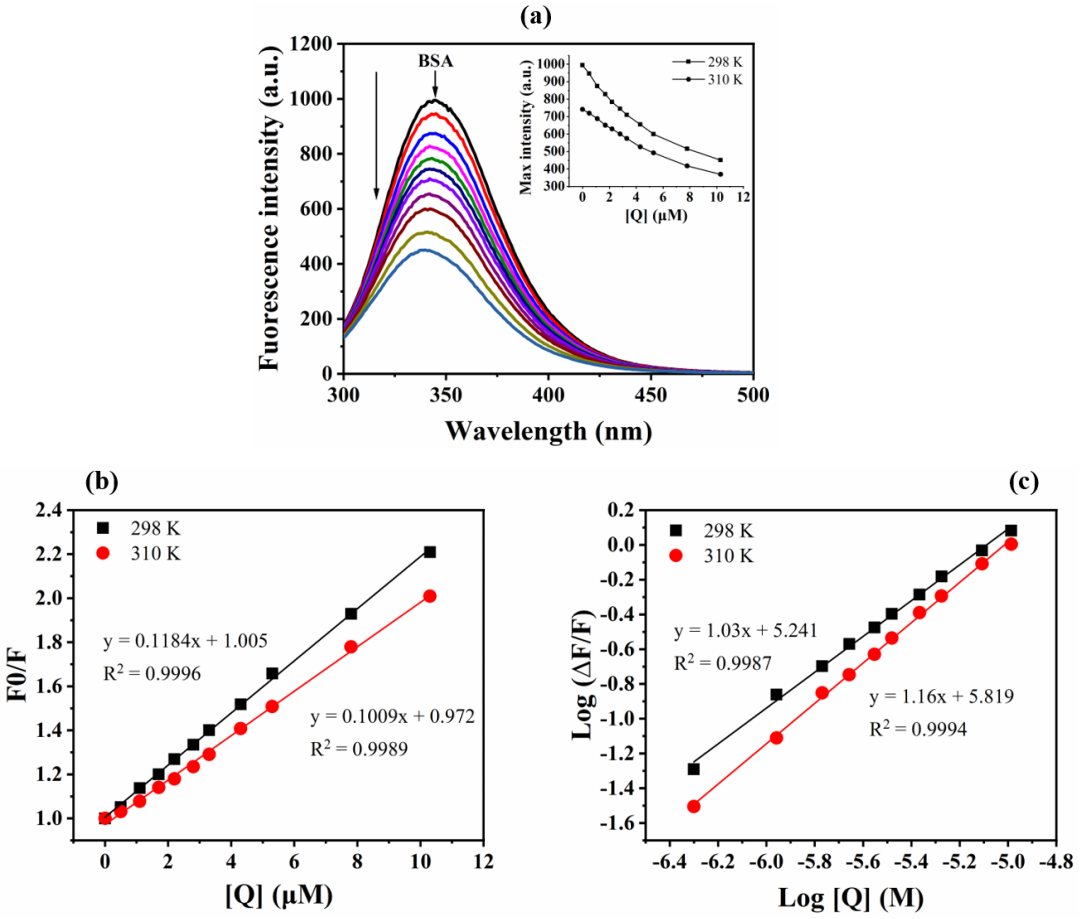

Fig. 2. (a) Fluorescence emission spectra of BSA (1.5 μM) in the absence and presence of BMC (concentrations of 0.5, 1, 1.5, 2, 2.5, 3, 4, 5, 7.5 and 10 μM) at λ_{ex}=280 nm at 298 K. (b) Stern–Volmer plots for quenching of BSA by BMC at temperatures of 298 and 310 K. (c) The plot of log (ΔF/F) versus log [Q] obtained from quenching of BSA by BMC at temperatures of 298 and 310 K.

RESULTS AND DISCUSSION

Molecular interaction study

One of the effective techniques for analyzing the small molecules and proteins such as albumin interactions, is fluorescence spectroscopy. Fluorescence emission of BSA is attributed to aromatic residues of Trp, Tyr and Phe (29, 30). Due to the low quantum yield of Tyr and Phe, mainly Trp is involved in the intrinsic fluorescence emission of BSA. Pursuant to the literature, fluorescence quenching, any process in which the fluorescence intensity of a protein is reduced, could be helpful for determining the interaction between a small molecule as a ligand and the protein (31). In this regard, the effect of BMC on the fluorescence intensity of BSA was determined in the absence and presence of different concentrations of BMC. The spectra in Fig. 2a shows a significant decrease in BSA fluorescence intensity with the increase of BMC concentration. This indicates that BMC has the ability to bind to BSA and quench the intrinsic fluorescence of Trp by changing the conformation of BSA or microenvironment around it. A variety of molecular interactions can lead this quenching, including excited state reactions, molecular rearrangements, ground state complex formation, energy transfer and collision quenching can lead this fluorescence quenching (32). In general, fluorescence quenching can occur through dynamic, static or both quenching mechanisms depending on the factors like temperature, viscosity, and diffusion coefficients (33). Accordingly, to determine the quenching mechanism, Stern–Volmer equation was employed. The Stern–Volmer plots based on F0/F versus [Q] at two studied temperatures are illustrated in Fig. 2b and the values of K_{SV} and k_q obtained from the slope of the fitted lines are shown in Table 1. The

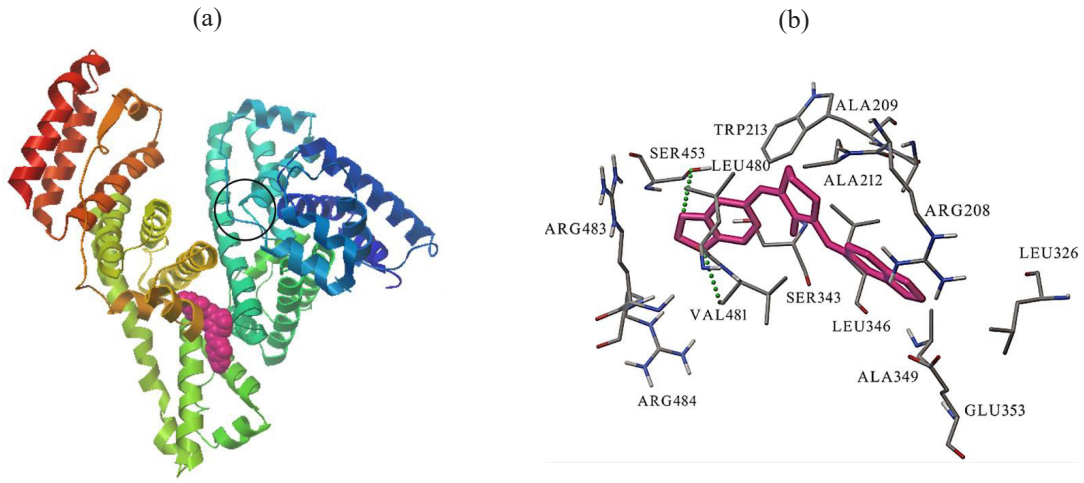

Fig. 3. Conformation with the lowest free energy obtained from molecular docking studies. (a) The BSA and BMC are represented by ribbon diagram and sphere model, respectively. (b) Amino acid residues surrounding BMC within A°.

plots show good linearity, and according to the results, increasing the temperature from 298 to 310 K, the values of K_{SV} decreased, indicating static mechanism for quenching. Also, higher values of k_q compared to maximum scattering collision quenching constant (2.0×10^{10}) demonstrated the static mechanism of quenching as well. Moreover, the values of binding constant (K_b) and binding sites (n) calculated from Eq. 2 and Fig. 2c are shown in Table 1. The approximate equality of n to 1 values demonstrated that one binding site is available on the BSA for BMC molecule. As well, higher K_b value at 310 K than 298 K demonstrated the increasing of bonding affinity of BSA to BMC with temperature increment. Moreover, previous studies have shown that four non-covalent interaction forces including electrostatic force, hydrophobic interactions, hydrogen bonds, and van der Waals forces, may occur between small molecules and macromolecules (34). Interaction forces mode can be confirmed using thermodynamic parameters (ΔH° and ΔS°), so that if ΔH° < 0 and ΔS° > 0, the electrostatic forces; ΔH° > 0 and ΔS° > 0, hydrophobic interactions; ΔH° < 0 and ΔS° < 0 van der Waals interactions and hydrogen bonds are more dominant binding forces (28). According to this, thermodynamic parameters were obtained using Van't Hoff and standard Gibbs free energy (ΔG°) equations (Eq. 3 and Eq. 3) and presented in Table 1. Both ΔH° and ΔS° showed values above zero, indicating a predominant hydrophobic interaction between BSA and BMC. Also, negative values for ΔG° showed that the reaction of BSA and BMC was spontaneous.

Subsequently, molecular docking investigations were performed to supplement fluorescence spectroscopy studies and for further understanding of BSA protein and BMC interactions. Previously, subdomains IIA and IIIA are known as the main binding sites of albumin for small molecules. On the other hand, curcumin and its derivatives have shown an affinity to bind to hydrophobic cavity of albumin in subdomain IIA close to Trp-213 residue (35-38). Hence, our docking studies focused on subdomain IIA of BSA. The results showed that BMC successfully binds to the subdomain IIA in the interface of subdomain IIB and in the vicinity of Trp-213. This result also justified Trp fluorescence quenching of BSA in the presence of BMC. The best energy-ranked conformation with the lowest free energy (ΔG°) of -6.59 kcal/mol and lowest RMSD value (0.0) is shown in Fig. 3. The ΔG° value in confirming the values obtained from thermodynamic parameters is negative and indicates spontaneous reaction. However, the difference with the experimental value (-11.28 kcal/mol) can be due to ignoring the presence of solvent and/or rigidity of some other residues of BSA in the docking studies (26). Moreover, BMC was surrounded by a number of amino acid with abundance of hydrophobic residues of Val-481, Leu-480, Trp-213, Ala-209, Ala-212, Lue-346, Ala-349, Leu-362, polar residues of Ser-453 and Ser-343, and charged residues of Arg-483, Arg-484, Arg-208 and Glu-353. Also, two hydrogen bonds were formed between BMC and Val-481 and Ser-453 residues of

Table 1. Binding and thermodynamic parameters of the interaction between BSA and BMC at two temperatures of 298 and 310 K obtained from fluorescence spectroscopy studies.

T (K)	$K_{sv} \times 10^5$ (M^{-1})	$kq \times 10^{13}$ ($M^{-1}S^{-1}$)	R^2	$K_b \times 10^8$ (M^{-1})	n	R^2	ΔG (kJ/mol)	ΔH° (kJ/mol)	ΔS° (kJ/mol.K)
298	1.184 ± 0.001	1.184	0.9996	1.889 ± 0.105	1.03	0.9973	-47.22 ± 2.25	+ 3.698	+ 0.2825
310	1.009 ± 0.001	1.009	0.9989	3.366 ± 0.078	1.16	0.9994	-50.61 ± 2.55		

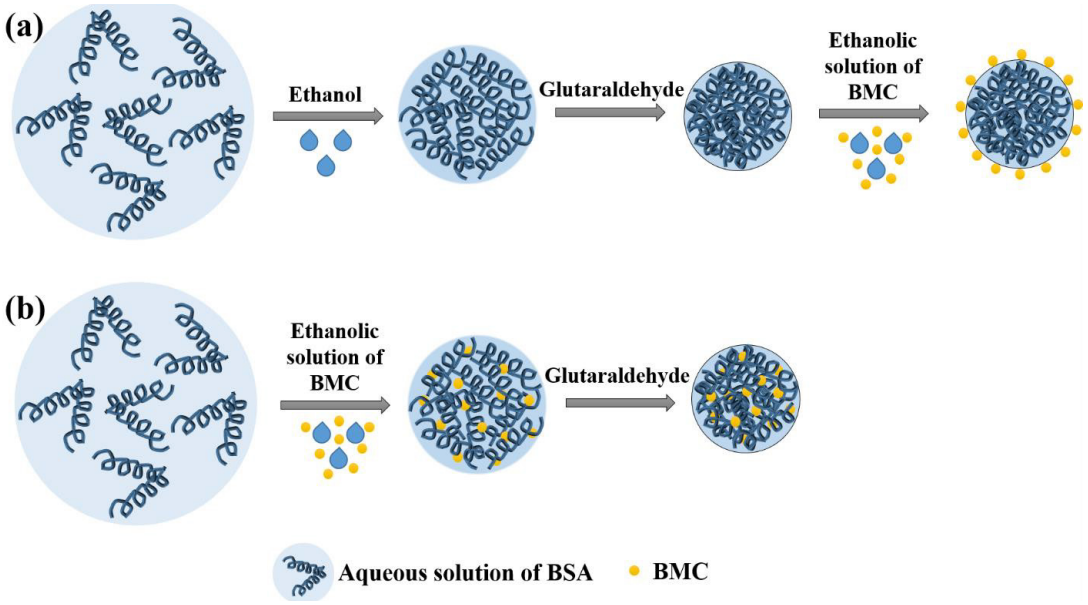

Fig. 4. Schematic of the BSANPs synthesis and BMC loading procedures based on desolvation method through, (a) adsorption (b) entrapment approaches

BSA (Fig. 3b). Therefore, the predominant binding between BSA and BMC is hydrophobic interaction followed by hydrogen bonds which is in consistent with thermodynamic parameters studies.

Preparation of BMC loaded BSANPs

Desolvation is a thermodynamically driven self-assembly technique used for preparing albumin NPs and loading both hydrophilic and hydrophobic anticancer drugs such as doxorubicin, docetaxel, curcumin, etc. (39-41). In various studies, drug loading has been performed in different approaches. Sun et al. after synthesizing the albumin NPs, loaded doxorubicin by adding the drug to the NPs solution and stirring it for a specified duration of time (42). Also, Fattahian Kalhor et al. with the aim of loading one of the curcumin derivatives (DVH) on albumin NPs by desolvation method, first synthesized NPs, then added the drug solution to the NPs solution and stirred it continuously for a period of time (43). On the other hand, Salehiabar et al. loaded curcumin in albumin NPs during the synthesis of NPs and in the step of adding acetone desolvating agent containing curcumin (44). Furthermore, loading the CDF derivative of curcumin on albumin NPs was done by Gawde et al. simultaneously as the NPs preparing (45). In the present study, two different loading approaches based on the desolvation method were used to investigate the effect of loading process on properties of drug-loaded NPs. In adsorption approach, first BSANPs were synthesized using ethanol as desolvating agent and glutaraldehyde as crosslinker, and in the next step by continuous stirring of the NPs aqueous solution and the ethanolic solution of BMC for a period of time the drug was loaded onto the NPs. In the entrapment method on the other hand, loading was performed simultaneously with the synthesis of BSANPs in the step of adding

Table 2. Physicochemical properties of BSANPs, BMC@BSANPs-A and BMC@BSANPs-E

Synthesis method	BMC/BSA (w/w)	DL %	EE %	Particle Size	PDI	Zeta Potential
Adsorption	1:40	8.64 ± 0.34	80.90 ± 0.49	195.4 ± 3.11	0.155 ± 0.08	-34.7 ± 0.91
	1:20	17.44 ± 0.64	84.08 ± 0.29	196.0 ± 1.89	0.052 ± 0.02	-38.9 ± 0.20
	1:10	37.99 ± 0.45	84.03 ± 0.23	201.7 ± 1.57	0.037 ± 0.03	-46.5 ± 0.64
Entrapment	1:40	7.94 ± 0.16	83.27 ± 0.37	161.3 ± 1.32	0.123 ± 0.07	-33.2 ± 0.72
	1:20	16.13 ± 0.30	88.18 ± 0.28	159.2 ± 3.45	0.135 ± 0.03	-41.2 ± 0.38
	1:10	35.62 ± 0.57	91.93 ± 0.51	165.7 ± 2.76	0.105 ± 0.05	-58.4 ± 0.26
Blank	BSANPs			171.1 ± 2.55	0.09 ± 0.03	-31.3 ± 0.75

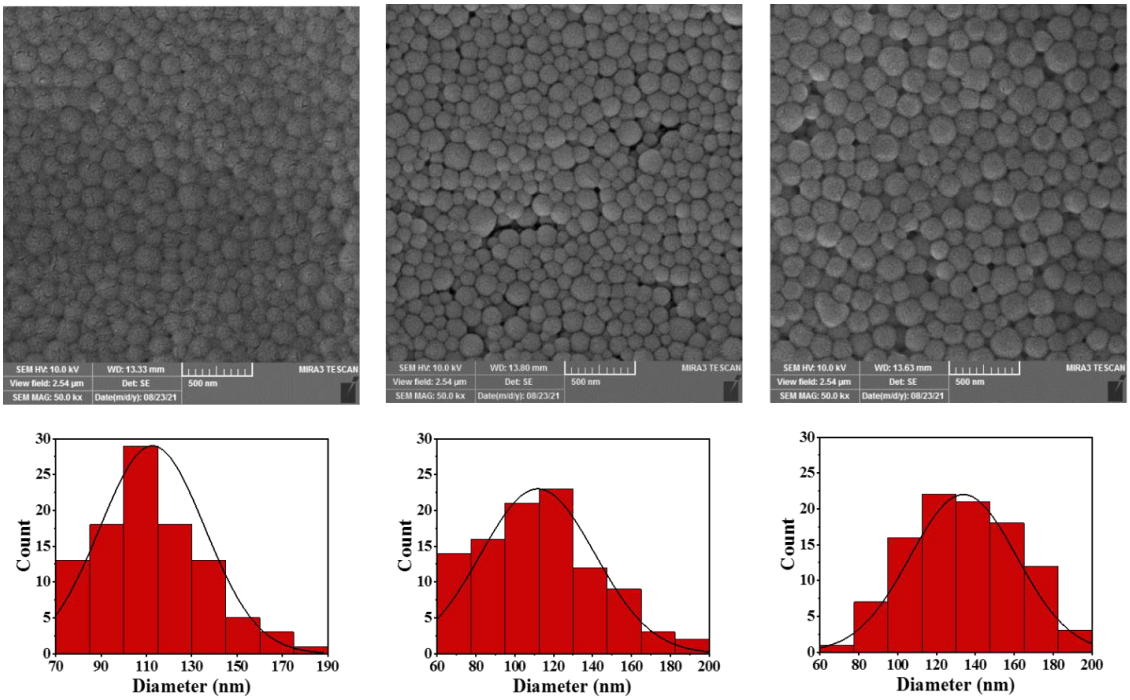

Fig. 5. FESEM images using secondary electrons mode at 50 kx magnification and particle size distribution histograms. (a) BSANPs, (b) BMC@BSANPs-E, (c) BMC@BSANPs-A

the ethanol containing the dissolved BMC. Considering the addition of drug molecules after complete formation of BSANPs in the adsorption method, it seemed that the BMC had attached to binding sites on the surface of BSANPs. However, in the entrapment method, due to the addition of the drug before the formation of BSANPs and its fixation with glutaraldehyde, BMC had entrapped within the protein network of NPs in addition to formation bonds to it. Fig. 4. illustrates the schematic of the two synthesis and loading procedures.

Physicochemical characterization

Physicochemical charactristics of BSANPs, BMC@BSANPs-A and BMC@BSANPs-E formulations with different BMC/BSA ratios are shown in Table 2. The size of NPs plays a major role in their biodistribution and delivery to cancereous cells. According to the results of this study, the hydrodynamic particle size of the formulations was in the range of 159.2 ± 3.45 to 201.7 ± 1.57 nm (Fig. S3). As previously reported, nanoparticles with a size range between 100 to 200 nm can circulate in the bloodstream for a

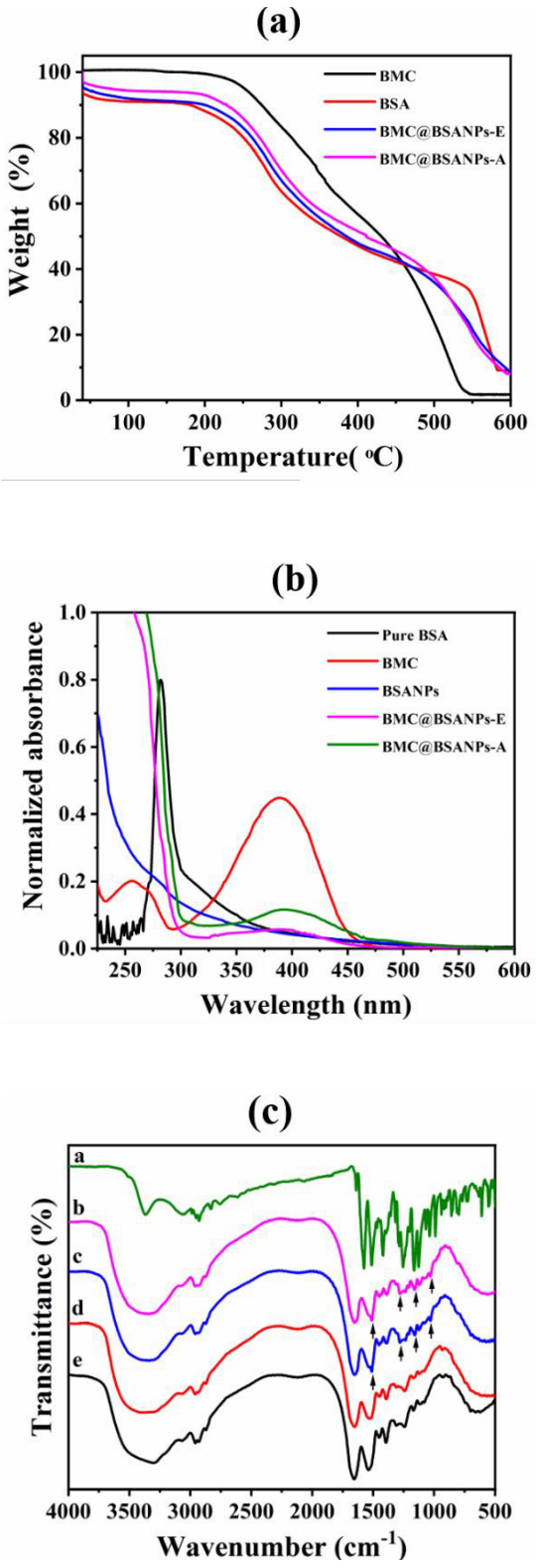

Fig. 6. (a) UV-Vis spectra, (b) TGA thermogram, (c) FTIR spectra of a BMC, b BMC@BSANPs-A, c BMC@BSANPs-E, d BSANPs and e BSA

longer period of time. Actually, this size range of NPs facilitates interlization into cells via receptor-mediated endocytosis, while larger ones undergo phagocytosis, and the smaller size of NPs may lead to their renal removal (46, 47). It has also been indicated that NPs of this size range can extravasate through the endothelial fenestration of tumors and accumulate in the tumor environment due to EPR effect (48). For both BMC@BSANPs-A and BMC@BSANPs-E, with increasing BMC/BSA ratio from 1:40 to 1:20, the average particle size did not change significantly ($p > 0.05$), but at the ratio of 1:10, average particle size increased significantly ($p < 0.05$). Likewise, in studies on the loading of paclitaxel and curcumin on albumin nanoparticles similar results have been reported (41, 49, 50). In addition, for all BMC/BSA ratios, BMC@BSANPs-E had smaller size than BMC@BSANPs-A. PDI values also indicated that the prepared formulations had a narrow size distribution. Meanwhile, zeta potential is an important parameter that indicates the surface charge and stability of NPs under colloidal conditions. NPs with zeta potential of more than ±30 show good colloidal stability due to surface charge repulsion (51). In addition, the negative surface charges of NPs lead to less toxicity as well as increase the circulation time due to the reduction of the chance of activating the immune system or opsonization and removal of NPs in the bloodstream (45, 52). According to the results of the present study, the zeta potential for all formulations had acceptable negative values, which indicated the good physical and electrostatic stability of prepared formulations (Fig. S4). The zeta potential values of BMC@BSANPs-E formulation were more negative than BMC@BSANPs-A, may be due to the smaller size of BMC@BSANPs-E which lead to higher specific surface and higher number of negative charged amino acids on NPs surface at neutral pH. In addition, increasing the BMC/BSA ratio enhanced the DL% in both formulations, which has been reported in similar studies on albumin NPs as nanocarrier (49, 53). Also, the DL% for the BMC@BSANPs-A in all ratios was slightly higher than that of BMC@BSANPs-E ($p < 0.05$), indicating that the amount of drug molecules attached to the surface of BSANPs was relatively higher than that of entrapped in the protein matrix. Since the NPs in the BMC@BSANPs-E formulation had smaller sizes, less drug may have been loaded in these NPs. On the other hand, EE% of BMC@BSANPs-E increased with rising BMC/BSA and reached

Table 3. Assigned protein bands in FTIR spectra of BSA and nano-formulations

Assigned band (cm^{-1})	O-H stretching	Amide A	Amide B	Amide I	Amide II	CH_2 bending	Amide III
BSA	3306	3068	2961	1654	1539	1395	1242
BSANPs	3325	3065	2961	1652	1531	1393	1243
BMC@BSANPs-E	3339	3080	2959	1654	1535	1389	1234
BMC@BSANPs-A	3345	3074	2961	1654	1512	1386	1234

to 91.93 ± 0.62 at 1:10 ratio, while for BMC@BSANPs-A, increasing the ratio from 1:40 to 1:20, EE% reached to 84.08 ± 0.35, but at 1:10, EE% remained almost constant. This illustrated that the BMC@BSANPs-E formulation had a greater capacity for encapsulating the drug molecules.

Fig. 5 shows the FESEM images of BSANPs, BMC@BSANPs-A and BMC@BSANPs-E at 50 kx magnification and the particle size distribution histogram obtained using ImageJ.JS. According to these data and TEM images in Fig. S5, the NPs had a spherical morphology with smooth surfaces and a proper size distribution. The mean particle sizes for BSANPs, BMC@BSANPs-E and BMC@BSANPs-A were obtained 112.03 ± 1.04 nm, 109.68 ± 1.72 nm and 133.97 ± 2.00 nm, respectively. Although the ratio of loaded drug in two formulations was the same, the BMC@BSANPs-A had a larger particle size than BMC@BSANPs-E which was consistent with the results of the DLS analysis. However, it should be noted that in DLS analysis, the hydrodynamic diameter of NPs is measured in aqueous medium and the presence of water molecules cause swelling and increasing of the size of NPs while FESEM imaging is performed on dried samples. Therefore, the size of NPs obtained from FESEM images are smaller than DLS analysis.

UV-Vis spectroscopy was used for structural studies. Absorption spectra of BSA, BMC and formulations are shown in Fig. 6a. The characteristic peak for BSA was obtained at 283 nm that was related to the amino acids with aromatic rings specifically tryptophan absorbance (54). This peak disappeared in NPs spectra, which could be due to the crosslinking of amino acids and/or entrapment of related functional groups into the NPs (13, 42). As well, in the absorption spectrum of BMC, two characteristic peaks were detected at 256 nm and 389 nm. However, peak at 389 nm was considered as the characteristic peak due to the higher intensity. This peak with lower intensity was also observed in the BMC@BSANPs-A and BMC@BSANPs-E spectra which could be related to BMC molecules adsorbed on the surface of nanoparticles.

The thermograms of TGA analysis, shown in Fig. 6b, illustrated that BSA, BMC@BSANPs-E and BMC@BSANPs-A had an initail weight loss of 9.13%, 8.77% and 5.95% up to about 160℃, respectively, which was attributed to water loss. For BMC, however, no significant initial weight loss was observed, which may be due to its hydrophobic nature. Thermal decomposition of BMC occurred with a relatively rapid rate beginning from 182℃ and reaches a total weight loss of 97.5% up to 570℃. Also the BSA showed total weight loss about 81.77%, with decomposition beginning from 160℃. For BMC@BSANPs-A and BMC@BSANPs-E decomposition began from about 162℃ and 173℃, respectively, which both were more than of BSA due to BMC loading in BSANPs. In addition, total weight loss up to 600℃ for BMC@BSANPs-A and BMC@BSANPs-E were obtaind 84.3% and 80.18%, respectively. As it turned out, both NPs had a slower decomposition rate than free BMC. However, BMC@BSANPs-A showed higher total weight loss, as well as higher onset of decomposition temperature, may be due to the more BMC loaded on the surface of NPs (Table 2).

Furthermore, FTIR spectra were obtained for more structural changes evaluations and confirmation of drug loading in NPs. As shown in Fig. 6c, the absorption peaks of the pure BSA at 3306 cm^{-1}, 3068 cm^{-1}, 2961 cm^{-1}, 1654 cm^{-1}, 1539 cm^{-1}, 1395 cm^{-1} and 1242 cm^{-1} were related to O-H stretching vibrations, amide A (N-H stretching vibrations), amide B (N-H stretching vibrations of free ion NH_3^+), amide I (C=O stretching vibrations), amide II (C-N stretching and N-H bending vibrations), CH_2 bending vibrations, and amide III (C-N stretching vibrations and N-H bending vibrations) (40, 55, 56). On the other hand, according to Table 3, the BSANPs,

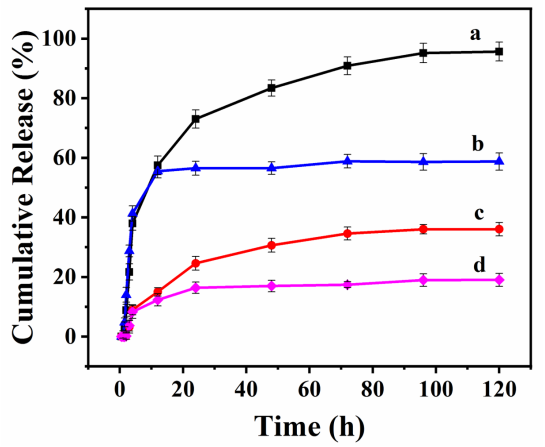

Fig. 7. Cumulative release profiles of (a) BMC@BSANPs-A at pH 5.5, (b) BMC@BSANPs-A at pH 7.2, (c) BMC@BSANPs-E at pH 5.5 and (d) BMC@BSANPs-E at pH 7.2

BMC@BSANPs-E, and BMC@BSANPs-A spectra showed protein amide bands with slight shifts and a decrease in intensity of peaks compared to the pure BSA, indicating a change in CN or NH bands due to interactions of albumin different groups and changes in the secondary structure of protein during crosslinking with glutaraldehyde and interaction with BMC (54, 57). Also, in the FTIR spectrum of BMC, the absorbtion peak at 3366 cm^{-1} corresponded to the stretching vibrations of O-H bonds, the peaks in the range of 3049 cm^{-1} to 2613 cm^{-1} were due to aromatic and aliphatic C-H stretching vibrations and the peaks at 1640 cm^{-1}, 1576 cm^{-1} and 1512 cm^{-1} were due to C=O and aromatic C=C stretching vibrations. In addition, absorbtion at 1420 cm^{-1} was due to olephinic bending C-H vibration and strong peaks in the range of 1255 cm^{-1} to 990 cm^{-1} were related to aromatic C-O strething vibrations and C-O-C strething vibrations of methylenedioxy groups. Peaks in the range below 900 cm^{-1} were also caused by aromatic C-H out of plane bending vibrations (58-61). In the BMC@BSANPs-E and BMC@BSANPs-A FTIR spectra, most of the pure BMC peaks were overlapped by BSA peaks, nevertheless the presence of 1512 cm^{-1}, 1261 cm^{-1}, 1160 cm^{-1} and 1031 cm^{-1} peaks of BMC indicated the successful loading of BMC into BSANPs.

In-vitro drug release study

The release of BMC from BMC@BSANPs-A and BMC@BSANPs-E was studied at pH 5.5 and 7.2. Fig. 7 shows the percentage of cumulative release of formulations over time. According to these results, BMC released from BSANPs in a biphasic pattern in all samples. The burst release was observed at the first 4 h which was subsequently followed by a controlled release process. Accordingly, in the first phase, the release percentage for BMC@BSANPs-A at 5.5 and 7.2 pH was 38% and 41% and for BMC@BSANPs-E was 9% and 8%, respectively. This initial rapid release was probably due to the desorption of drug molecules that were weakly attached to the NPs surfaces through hydrophobic interasctions. Sustained release in the next phase may be due to the desorption of the more strongly attached molecules or the ones have partially migrated and trapped into the protein matrix during the loading process of BMC@BSANPs-A or due to the difussion of the drug molecules entrapped into the NPs matrix during the preparation and loading process of BMC@BSANPs-E (43, 62). On the other hand, BMC release from NPs was highly dependent on pH and loading method. Accordingly, the maximum released drug from BMC@BSANPs-A after 120 h at pH 5.5 and 7.2 was 96% and 59%, while this value for BMC@BSANPs-E was 34% and 19%, respectively. It should be noted that crosslinking with glutaraldehyde in desolvation method plays an important role in degradation and subsequent release behavior of BSANPs (62). Actually for BMC@BSANPs-A, BMC was loaded after formation of NPs and stabilization by glutaraldehyde, therefore, the BMC molecules may have been mainly adsorbed on the NPs. Thus, during release, the adsorbed molecules are easily separated from the surface of the NPs. On the other hand, in BMC@BSANPs-E, the BMC was added at the NPs formation stage and then the NPs and drug molecules were fixed together by crosslinker. So, most of the BMC molecules were entrapped and only a small amounts were able to diffuse from the NPs matrix and release into the medium. Comparable results have been reported in a study by Merodio et al. and Sadeghi et al. on the loading of albumin NPs with ganciclovir and curcumin, respectively (63, 64). Despite the lower *in-vitro* release of BMC from BMC@BSANPs-E, it can be expected that *in-vivo* administration of this formulation prevents rapid metabolism of BMC and reduces drug leakage in the bloodstream which can lead to fewer side effects for normal cells. Moreover, the active and passive targeting ability of albumin NPs, leads to delivery of drug cargo to the tumor site where BMC@BSANPs-E

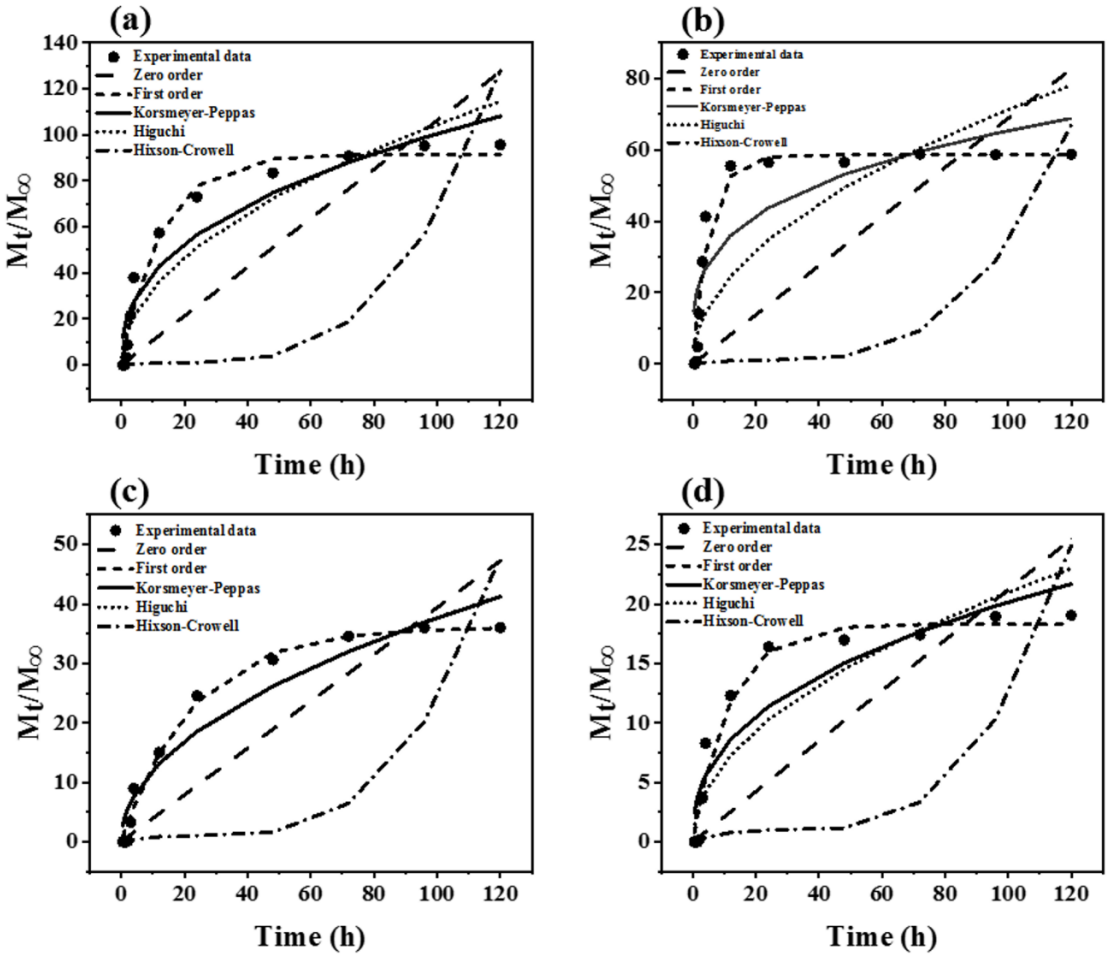

Fig. 8. Release data fitting with different kinetic models. (a) BMC@BSANPs-A pH 7.2, (b) BMC@BSANPs-A pH 5.5, (c) BMC@BSANPs-E pH 7.2, (d) BMC@BSANPs-E pH 5.5.

can gradually release all the entrapped BMC due to enzymatic degradation of albumin. In addition, both formulations showed greater release rates in acidic pH than neutral condition which could be caused by degradation of the bonds between albumin and BMC as well as degradation of the protein matrix in acidic conditions (63). Compared to the neutral pH of the blood, the tumor sites as well as the endosomes and lysosomes of the cells have an acidic pH (4.5-6.0). Thus, greater release in acidic conditions can reduce the adverse effects of drugs on normal cells during circulation and aid in the targeted release of the drug in the tumor sites (41, 44, 65)

Relaese kinetic study

To determine the release mechanism of the BMC from BMC@BSANPs-A and BMC@BSANPs-E at pH 5.5 and 7.2, the cumulative release data were fitted to different mathmatical kinetic models (Fig. 8). Nonlinear regression method was used for this purpose. The results including the kinetic parameters and values of the coefficient of determination (R^2) are shown in Table 4. R^2 coefficient indicates the goodness of the model and when it is equal to 1, the obtained data are completely fitted to model. According to the results of Table 4, the first order kinetic model had the closest values of R^2 to 1 for all the studied samples. Thus, the release of BMC from BSANPs followed a first order kinetic model. According to this model, the amount of

released drug depends on the concentration gradient of drug between the static fluid layer around the carrier surface and the release medium. In this model, it is assumed that the surface of the

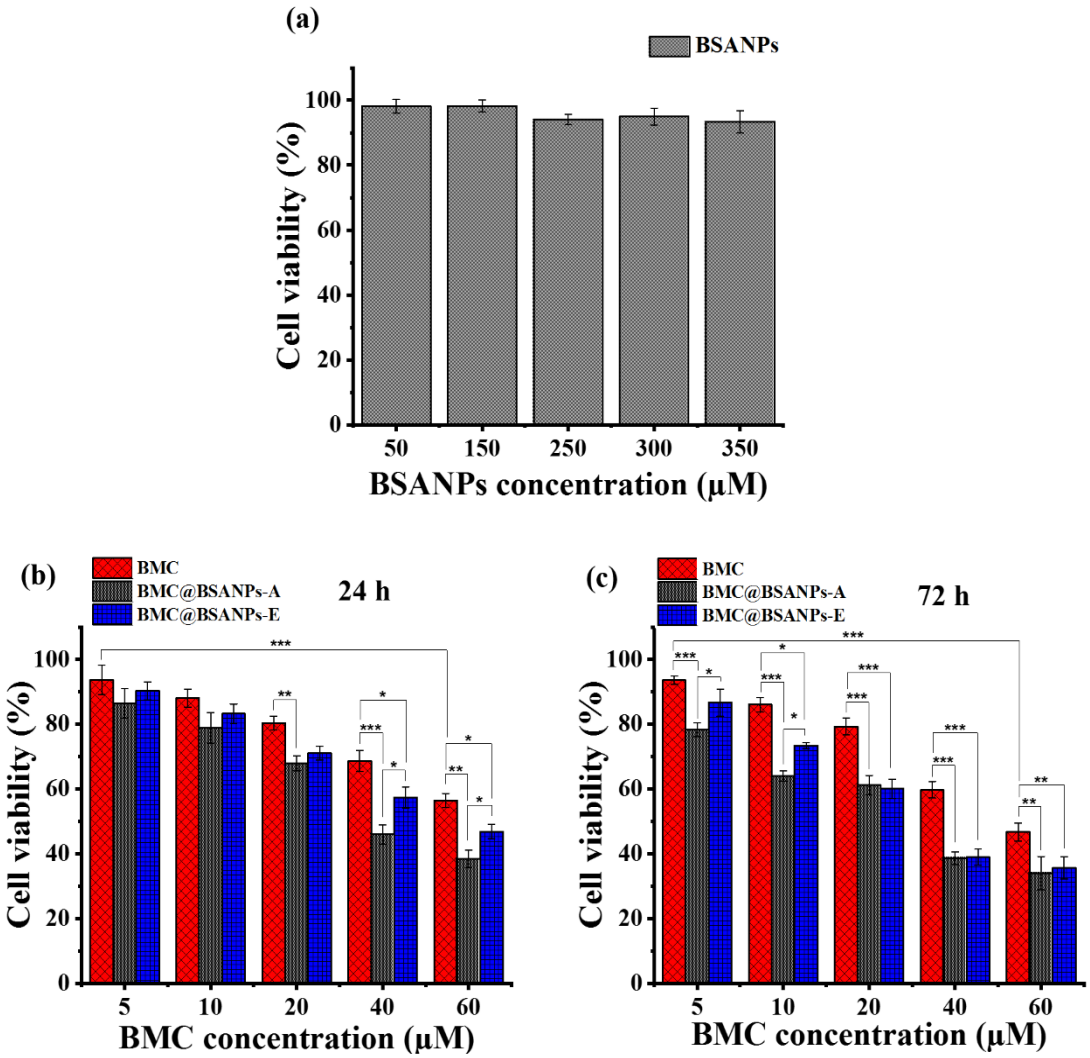

Fig. 9. *In-vitro* cytotoxicity of BSANPs after 72h (a), BMC, BMC@BSANPs-A and BMC@BSANPs-E after 24h (b), BMC, BMC@BSANPs-A and BMC@BSANPs-E after 72h incubation (c) against MCF-7 cells. Data are presented as mean ± SD of three experiments. *: $p < 0.05$, **: $p < 0.01$, ***: $p < 0.001$."

carrier remains constant and does not change its shape during release. This result meant that the release of BMC from BSANPs was not mainly due to the degradation of the protein network that could lead to its surface change or deformation. On the other hand, the value of n obtained from the Korsmeyer-Peppas model, which indicates the diffusion coefficient, is less than 0.5 for the samples. Conforming to this model, if n <0.5: the fickian diffusion, 0.5 <n < 1: the irregular diffusion, n = 1: type II transfer and for higher n values: super type II transfer controls the release mechanism (66-68). Therefore, the release mechanism of BMC@BSANPs-A and BMC@BSANPs-E formulations was controlled by fickian diffusion. This mechanism could occur because of the chemical potential gradient of BMC molecules. Similar release mechanism was reported for the release of curcumin from two different albumin containing carriers including egg albumin NPs and albumin shell of magnetic nanohybrid particles (cluster@silica@albumin) (69, 70).

Cytotoxicity assay

The cytotoxicity of free BMC, BSANPs and BMC-containing BSANPs was investigated on MCF-7 cancer cell line using MTT assay. For this purpose, cells were incubated for 72 h with

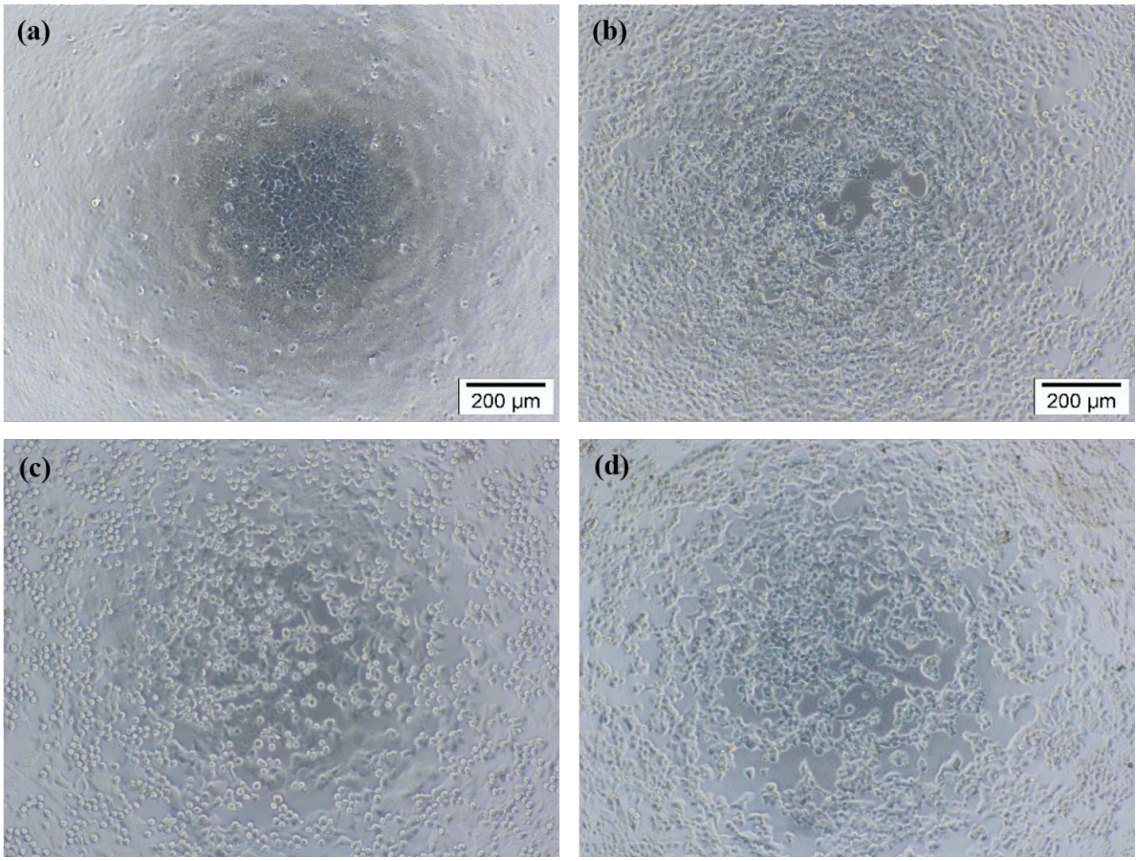

Fig. 10. Optical microscopy images of MCF-7 cells after 72 h, (a) Untreated cells, (b) The cells treated with BMC, (c) BMC@BSANPs-E and (d) BMC@BSANPs-A at the concentration of 20 µM

BSANPs samples at concentrations of 50, 150, 250, 300 and 350 µM. As shown in Fig. 9a, BSANPs did not show significant cytotoxicity against MCF-7 cells in the assessed concentrations ($p > 0.05$). Also, the cytotoxicity evaluation of free BMC as well as BMC@BSANPs-A and BMC@BSANPs-E with different concentrations of BMC (5, 10, 20, 40 and 60 µM) on MCF-7 cancer cells indicated the dependence of cell viability to BMC concentration and incubation time (Fig 9b and 9c). Increasing BMC concentration and incubation time from 24 to 72 h, significantly reduced the cell viability ($p < 0.05$). In addition, IC_{50} values, shown in Table 5, indicated the higher cytotoxicity and subsequently more efficient inhibition of cell growth and proliferation for BMC-containing BSANPs compared to free BMC. This further inhibitory effect of NPs could be due to increased endocytosis and cell uptake in the presence of albumin as an endogenous ligand, as well as sustained release of drug cargo by BSANPs (41, 61). The optical microscopy images in the Fig. 10 also showed that the cells treated with NPs had lower viability than those treated with free BMC (after 72 h incubation at the concentration of 20 µM), as well as the morphological changes and cell shrinkage were more evident in them. On the other hand, BMC@BSANPs-A showed more cytotoxicity than BMC@BSANPs-E after 24 h of incubation at concentration higher than 40 µM ($p < 0.05$). Considering the higher DL% (Table 2) and release behavior of BMC@BSANPs-A (Fig. 7), it can be concluded that in the first 24 h, more BMC release from the NPs surface resulted in higher cytoxicity. However, after 72 h of incubation, at concentrations equal to and greater than 20 µM, both formulations showed relatively similar cytoxicity ($p > 0.05$), although at lower concentrations BMC@BSANPs-A still showed higher toxicity compared to BMC@BSANPs-E ($p < 0.05$). This result could be due to the sustained release of BMC from BMC@BSANPs-E over a longer period of time as these NPs enters the cells and release their drug cargo via degradation of BSA.

Table 4. Release kinetic parameters obtained from data fitting with mathematical models

Formulation	Kinetics models														
	Zero order			First order			Korsmeyer-Peppas				Higuchi			Hixon-Crowell		
	k_0	R^2	S	k_1	a	R^2	S	k_{KP}	n	R^2	S	k_H	R^2	S	k_{HC}	R^2	S
BMC@BSANPs-A pH 5.5	1.0621	0.7300	0.1451	0.0794	91.5078	0.9778	0.04893	15.8171	0.4015	0.9132	0.1052	10.4561	0.8844	0.1089	0.050193	0.347168	0.2634
BMC@BSANPs-A pH 7.2	0.6884	0.4818	0.1959	0.1901	58.6293	0.9608	0.0712	17.4502	0.2856	0.7548	0.1987	7.1244	0.6597	0.1731	0.04198	0.19596	0.3016
BMC@BSANPs-E pH 5.5	0.3984	0.8102	0.1290	0.0441	36.1074	0.9905	0.0321	3.8497	0.4951	0.9406	0.0855	3.7713	0.9396	0.0859	0.038339	0.389297	0.2713
BMC@BSANPs-E pH 7.2	0.2121	0.6727	0.1666	0.0866	18.3010	0.9698	0.0597	3.1963	0.3998	0.8681	0.1348	2.0976	0.8356	0.1349	0.032325	0.320731	0.2937

Table 5. The IC_{50} values of BMC, BMC@BSANPs-A and BMC@BSANPs-E obtained from MTT assay against MCF-7 cells after 24 and 72 h incubation.

	IC_{50} (μM)	
time	24 h	72 h
BMC	67.31 ± 3.47	54.30 ± 2.16
BMC@BSANPs-A	42.23 ± 0.77	33.73 ± 0.68
BMC@BSANPs-E	51.64 ± 0.92	36.85 ± 2.54

CONCLUSION

In this study, fluorescence spectroscopy and molecular docking studies showed that the BMC has the affinity to bind to BSA and quench the Trp fluorescence, mainly through hydrophobic interactions. In addition, applying two adsorption and entrapment approaches, BMC loaded albumin nanoparticles were successfully prepared using desolvation method. Particle size and zeta potential of formulations were in the desirable range in terms of benefiting from EPR targeting and longer blood circulation time of drug. However, BMC@BSANPs-E had smaller particle size than BMC@BSANPs-A according to hydrodynamic particle size and microscopic measurements. Both formulations released more drug at acidic conditions. On the other hand, BMC@BSANPs-A released more drug at both pH which can be due to the ease of release of adsorbed molecules in this formulation in contrast to entrapping the drug molecules in the protein network in BMC@BSANPs-E. Also, the formulations follow the first-order kinetic model, and the release mechanism was controlled by fickian diffusion. The results of cytotoxicity against MCF-7 cancer line showed that despite the higher cytotoxicity of BMC@BSANPs-A in lower concentrations of BMC, after 72 h incubation, at higher concentrations, both formulations show relatively similar cytotoxicity and thus similar efficiency. Ultimately, according to the concluded results, loading of BMC in both formulations could improve its anti-cancer activity. However, due to its smaller size and less drug leakage probability, BMC@BSANPs-E formulation may be more useful for drug delivery applications.

ACKNOWLEDGMENT

This work was supported financially by the Department of Nanotechnology and Advanced Materials, Materials and Energy Research Center, Karaj, Iran, and Faculty of Pharmacy, Hormozgan University of Medical Sciences, Bandar Abbas, Iran. Authors are grateful for this support.

CONFLICT OF INTEREST

The authors declare no conflict of interest.

REFERENCES

1. Li L, Chen Y, Wang Q, Li Z, Liu Z, Hua X, et al. Albumin-encapsulated Nanoparticles of Naproxen Platinum(IV) Complexes with Inflammation Inhibitory Competence Displaying Effective Antitumor Activities in vitro and in vivo. Int J Nanomedicine. 2021;16:5513-29. https://doi.org/10.2147/IJN.S322688
2. Jiang M, Li S, Wu J, Li W, Wen XA, Liang H, et al. Designing biotin-human serum albumin nanoparticles to enhance the targeting ability of binuclear ruthenium(III) compound. J Inorg Biochem. 2021;215:111318. https://doi.org/10.1016/j.jinorgbio.2020.111318
3. Catanzaro G, Curcio M, Cirillo G, Spizzirri UG, Besharat ZM, Abballe L, et al. Albumin nanoparticles for glutathione-responsive release of cisplatin: New opportunities for medulloblastoma. Int J Pharm. 2017;517(1-2):168-74. https://doi.org/10.1016/j.ijpharm.2016.12.017
4. Abolhassani H, Shojaosadati SA. A comparative and systematic approach to desolvation and self-assembly methods for synthesis of piperine-loaded human serum albumin nanoparticles. Colloids and Surfaces B: Biointerfaces. 2019;184:110534. https://doi.org/10.1016/j.colsurfb.2019.110534
5. Aziz A, Sefidbakht Y, Rezaei S, Kouchakzadeh H, Uskoković V. Doxorubicin-loaded, pH-sensitive Albumin Nanoparticles for Lung Cancer Cell Targeting. Journal of Pharmaceutical Sciences. 2022;111(4):1187-96. https://doi.org/10.1016/j.xphs.2021.12.006
6. Karami K, Jamshidian N, Hajiaghasi A, Amirghofran Z. BSA nanoparticles as controlled release carriers for isophethalaldoxime palladacycle complex; synthesis, characterization, in vitro evaluation, cytotoxicity and release kinetics analysis. New Journal of Chemistry. 2020;44(11):4394-405. https://doi.org/10.1039/C9NJ05847H
7. Spada A, Emami J, Tuszynski JA, Lavasanifar A. The Uniqueness of Albumin as a Carrier in Nanodrug Delivery. Mol Pharm. 2021;18(5):1862-94. https://doi.org/10.1021/acs.molpharmaceut.1c00046
8. Kumari P, Paul M, Bobde Y, Soniya K, Kiran Rompicharla SV, Ghosh B, et al. Albumin-based lipoprotein nanoparticles for improved delivery and anticancer activity of curcumin for cancer treatment. Nanomedicine (Lond). 2020;15(29):2851-69. https://doi.org/10.2217/nnm-2020-0232
9. Kimura K, Yamasaki K, Nishi K, Taguchi K, Otagiri M. Investigation of anti-tumor effect of doxorubicin-loaded human serum albumin nanoparticles prepared by a desolvation technique. Cancer Chemother Pharmacol. 2019;83(6):1113-20. https://doi.org/10.1007/s00280-019-03832-3
10. Zhang B, Wan S, Peng X, Zhao M, Li S, Pu Y, et al. Human serum albumin-based doxorubicin prodrug nanoparticles with tumor pH-responsive aggregation-enhanced retention and reduced cardiotoxicity. Journal of Materials Chemistry B. 2020;8(17):3939-48. https://doi.org/10.1039/D0TB00327A
11. Weber C, Kreuter J, Langer K. Desolvation process and surface characteristics of HSA-

nanoparticles. Int J Pharm. 2000;196(2):197-200. https://doi.org/10.1016/S0378-5173(99)00420-2
12. Ahsan SM, Rao CM. The role of surface charge in the desolvation process of gelatin: implications in nanoparticle synthesis and modulation of drug release. Int J Nanomedicine. 2017;12:795-808. https://doi.org/10.2147/IJN.S124938
13. Tirkey B, Bhushan B, Uday Kumar S, Gopinath P. Prodrug encapsulated albumin nanoparticles as an alternative approach to manifest anti-proliferative effects of suicide gene therapy. Mater Sci Eng C Mater Biol Appl. 2017;73:507-15. https://doi.org/10.1016/j.msec.2016.12.108
14. Arroyo-Maya IJ, Hernández-Sánchez H, Jiménez-Cruz E, Camarillo-Cadena M, Hernández-Arana A. α-Lactalbumin nanoparticles prepared by desolvation and cross-linking: Structure and stability of the assembled protein. Biophysical Chemistry. 2014;193-194:27-34. https://doi.org/10.1016/j.bpc.2014.07.003
15. Iqbal H, Yang T, Li T, Zhang M, Ke H, Ding D, et al. Serum protein-based nanoparticles for cancer diagnosis and treatment. Journal of Controlled Release. 2021;329:997-1022. https://doi.org/10.1016/j.jconrel.2020.10.030
16. Chainoglou E, Hadjipavlou-Litina D. Curcumin analogues and derivatives with anti-proliferative and anti-inflammatory activity: Structural characteristics and molecular targets. Expert Opin Drug Discov. 2019;14(8):821-42. https://doi.org/10.1080/17460441.2019.1614560
17. Subramani PA, Panati K, Narala VR. Curcumin Nanotechnologies and Its Anticancer Activity. Nutr Cancer. 2017;69(3):381-93. https://doi.org/10.1080/01635581.2017.1285405
18. Razak NA, Akhtar MN, Abu N, Ho WY, Tan SW, Zareen S, et al. The in vivo anti-tumor effect of curcumin derivative (2E,6E)-2,6-bis(4-hydroxy-3-methoxybenzylidene)cyclohexanone (BHMC) on 4T1 breast cancer cells. RSC Advances. 2017;7(57):36185-92. https://doi.org/10.1039/C7RA06580A
19. Mirzaie Z, Reisi-Vanani A, Barati M, Atyabi SM. The Drug Release Kinetics and Anticancer Activity of the GO/PVA-Curcumin Nanostructures: The Effects of the Preparation Method and the GO Amount. Journal of Pharmaceutical Sciences. 2021;110(11):3715-25. https://doi.org/10.1016/j.xphs.2021.07.016
20. Santadkha T, Skolpap W, Thitapakorn V. Diffusion Modeling and In Vitro Release Kinetics Studies of Curcumin−Loaded Superparamagnetic Nanomicelles in Cancer Drug Delivery System. Journal of Pharmaceutical Sciences.
21. Zamrus SNH, Akhtar MN, Yeap SK, Quah CK, Loh W-S, Alitheen NB, et al. Design, synthesis and cytotoxic effects of curcuminoids on HeLa, K562, MCF-7 and MDA-MB-231 cancer cell lines. Chem Cent J. 2018;12(1):31-. https://doi.org/10.1186/s13065-018-0398-1
22. Wei X, Du ZY, Cui XX, Verano M, Mo RQ, Tang ZK, et al. Effects of cyclohexanone analogues of curcumin on growth, apoptosis and NF-κB activity in PC-3 human prostate cancer cells. Oncol Lett. 2012;4(2):279-84. https://doi.org/10.3892/ol.2012.710
23. Noureddin SA, El-Shishtawy RM, Al-Footy KO. Curcumin analogues and their hybrid molecules as multifunctional drugs. Eur J Med Chem. 2019;182:111631. https://doi.org/10.1016/j.ejmech.2019.111631
24. Alibeiki F, Jafari N, Karimi M, Peeri Dogaheh H. Potent anti-cancer effects of less polar Curcumin analogues on gastric adenocarcinoma and esophageal squamous cell carcinoma cells. Scientific Reports. 2017;7(1):2559. https://doi.org/10.1038/s41598-017-02666-4
25. Ramshini H, mohammad-zadeh M, Ebrahim-Habibi A. Inhibition of amyloid fibril formation and cytotoxicity by a chemical analog of Curcumin as a stable inhibitor. Int J Biol Macromol. 2015;78:396-404. https://doi.org/10.1016/j.ijbiomac.2015.04.038
26. Shahabadi N, Fili SM. Molecular modeling and multispectroscopic studies of the interaction of mesalamine with bovine serum albumin. Spectrochim Acta A Mol Biomol Spectrosc. 2014;118:422-9. https://doi.org/10.1016/j.saa.2013.08.110
27. Pawar SK, Jaldappagari S. Interaction of repaglinide with bovine serum albumin: Spectroscopic and molecular docking approaches. Journal of Pharmaceutical Analysis. 2019;9(4):274-83. https://doi.org/10.1016/j.jpha.2019.03.007
28. Lazniewska J, Agostino M, Hickey SM, Parkinson-Lawrence E, Stagni S, Massi M, et al. Spectroscopic and Molecular Docking Study of the Interaction between Neutral Re(I) Tetrazolate Complexes and Bovine Serum Albumin. Chemistry - A European Journal. 2021;27(44):11406-17. https://doi.org/10.1002/chem.202101307
29. Hosseini-Kharat M, Karami K, Saeidifar M, Rizzoli C, Zahedi-Nasab R, Sohrabijam Z, et al. A novel Pd(ii) CNO pincer complex of MR (methyl red): synthesis, crystal structure, interaction with human serum albumin (HSA) in vitro and molecular docking. New Journal of Chemistry. 2017;41(18):9897-907. https://doi.org/10.1039/C7NJ01415E
30. Xu H, Yao N, Xu H, Wang T, Li G, Li Z. Characterization of the interaction between eupatorin and bovine serum albumin by spectroscopic and molecular modeling methods. Int J Mol Sci. 2013;14(7):14185-203. https://doi.org/10.3390/ijms140714185
31. Mohammadgholi A, Leilabadi-Asl A, Divsalar A, Eslami-Moghadam M. Multi-spectroscopic studies of the interaction of new synthesized platin complex with human carrier protein of serum albumin. Journal of Biomolecular Structure and Dynamics. 2021;39(4):1506-11. https://doi.org/10.1080/07391102.2020.1745690
32. Jattinagoudar L, Meti M, Nandibewoor S, Chimatadar S. Evaluation of the binding interaction between bovine serum albumin and dimethyl fumarate, an anti-inflammatory drug by multispectroscopic methods. Spectrochimica Acta Part A: Molecular and Biomolecular Spectroscopy. 2016;156:164-71. https://doi.org/10.1016/j.saa.2015.11.026
33. Sun Y, Wei S, Yin C, Liu L, Hu C, Zhao Y, et al. Synthesis and spectroscopic characterization of 4-butoxyethoxy-N-octadecyl-1,8-naphthalimide as a new fluorescent probe for the determination of proteins. Bioorg Med Chem Lett. 2011;21(12):3798-804. https://doi.org/10.1016/j.bmcl.2011.04.026
34. Kazemi F, Divsalar A, Saboury AA. Binding Interaction of Glycated, Fructated and Native Human Hemoglobin with Bulk Propolis. Iranian Journal of Science and Technology, Transactions A: Science. 2021;45(3):785-93. https://doi.org/10.1007/s40995-021-01108-1
35. Matskou K, Kisaoglan B, Mavroidi B, Pelecanou M, Zoumpanioti M, Matis I, et al. Inducing the formation of a colloidal albumin carrier of curcumin. JCIS Open. 2022;6:100051.

https://doi.org/10.1016/j.jciso.2022.100051
36. Yang M, Wu Y, Li J, Zhou H, Wang X. Binding of Curcumin with Bovine Serum Albumin in the Presence of ι-Carrageenan and Implications on the Stability and Antioxidant Activity of Curcumin. Journal of Agricultural and Food Chemistry. 2013;61(29):7150-5. https://doi.org/10.1021/jf401827x
37. Mohammadi F, Bordbar A-K, Mohammadi K, Divsalar A, Saboury AA. Circular dichroism and fluorescence spectroscopic study on the interaction of bisdemethoxycurcumin and diacetylbisdemethoxycurcumin with human serum albumin. Canadian Journal of Chemistry. 2010;88(2):155-63. https://doi.org/10.1139/V09-169
38. Sahoo BK, Ghosh KS, Dasgupta S. Investigating the binding of curcumin derivatives to bovine serum albumin. Biophys Chem. 2008;132(2-3):81-8. https://doi.org/10.1016/j.bpc.2007.10.007
39. Kimura K, Yamasaki K, Nakamura H, Haratake M, Taguchi K, Otagiri M. Preparation and in Vitro Analysis of Human Serum Albumin Nanoparticles Loaded with Anthracycline Derivatives. Chemical & pharmaceutical bulletin. 2018;66(4):382-90. https://doi.org/10.1248/cpb.c17-00838
40. Ertugen E, Tunçel A, Yurt F. Docetaxel loaded human serum albumin nanoparticles; synthesis, characterization, and potential of nuclear imaging of prostate cancer. Journal of Drug Delivery Science and Technology. 2020;55:101410. https://doi.org/10.1016/j.jddst.2019.101410
41. Saleh T, Soudi T, Shojaosadati SA. Aptamer functionalized curcumin-loaded human serum albumin (HSA) nanoparticles for targeted delivery to HER-2 positive breast cancer cells. International Journal of Biological Macromolecules. 2019;130:109-16. https://doi.org/10.1016/j.ijbiomac.2019.02.129
42. Sun S, Xiao Q-R, Wang Y, Jiang Y. Roles of alcohol desolvating agents on the size control of bovine serum albumin nanoparticles in drug delivery system. Journal of Drug Delivery Science and Technology. 2018;47:193-9. https://doi.org/10.1016/j.jddst.2018.07.018
43. Fattahian Kalhor N, Saeidifar M, Ramshini H, Saboury AA. Interaction, cytotoxicity and sustained release assessment of a novel anti-tumor agent using bovine serum albumin nanocarrier. J Biomol Struct Dyn. 2020;38(9):2546-58. https://doi.org/10.1080/07391102.2019.1638303
44. Salehiabar M, Nosrati H, Javani E, Aliakbarzadeh F, Kheiri Manjili H, Davaran S, et al. Production of biological nanoparticles from bovine serum albumin as controlled release carrier for curcumin delivery. Int J Biol Macromol. 2018;115:83-9. https://doi.org/10.1016/j.ijbiomac.2018.04.043
45. Gawde KA, Kesharwani P, Sau S, Sarkar FH, Padhye S, Kashaw SK, et al. Synthesis and characterization of folate decorated albumin bio-conjugate nanoparticles loaded with a synthetic curcumin difluorinated analogue. J Colloid Interface Sci. 2017;496:290-9. https://doi.org/10.1016/j.jcis.2017.01.092
46. Yu X, Di Y, Xie C, Song Y, He H, Li H, et al. An in vitro and in vivo study of gemcitabine-loaded albumin nanoparticles in a pancreatic cancer cell line. International journal of nanomedicine. 2015;10:6825-34. https://doi.org/10.2147/IJN.S93835
47. Zhang N, Xia Y, Guo X, Wang P, Yan S, Lu C, et al. Preparation, characterization, and in vitro targeted delivery of folate-conjugated 2-methoxyestradiol-loaded bovine serum albumin nanoparticles. Journal of Nanoparticle Research. 2014;16(5):2390. https://doi.org/10.1007/s11051-014-2390-6
48. Kim B, Seo B, Park S, Lee C, Kim JO, Oh KT, et al. Albumin nanoparticles with synergistic antitumor efficacy against metastatic lung cancers. Colloids Surf B Biointerfaces. 2017;158:157-66. https://doi.org/10.1016/j.colsurfb.2017.06.039
49. Zhang S, Asghar S, Yu F, Chen Z, Hu Z, Ping Q, et al. BSA Nanoparticles Modified with N-Acetylcysteine for Improving the Stability and Mucoadhesion of Curcumin in the Gastrointestinal Tract. Journal of Agricultural and Food Chemistry. 2019;67(33):9371-81. https://doi.org/10.1021/acs.jafc.9b02272
50. Jiang L, Xu Y, Liu Q, Tang Y, Ge L, Zheng C, et al. A nontoxic disulfide bond reducing method for lipophilic drug-loaded albumin nanoparticle preparation: Formation dynamics, influencing factors and formation mechanisms investigation. International Journal of Pharmaceutics. 2013;443(1):80-6. https://doi.org/10.1016/j.ijpharm.2012.12.035
51. Bhattacharjee S. DLS and zeta potential - What they are and what they are not? J Control Release. 2016;235:337-51. https://doi.org/10.1016/j.jconrel.2016.06.017
52. Azizi M, Ghourchian H, Yazdian F, Bagherifam S, Bekhradnia S, Nyström B. Anti-cancerous effect of albumin coated silver nanoparticles on MDA-MB 231 human breast cancer cell line. Scientific Reports. 2017;7(1):5178. https://doi.org/10.1038/s41598-017-05461-3
53. Zu Y, Zhang Y, Zhao X, Zhang Q, Liu Y, Jiang R. Optimization of the preparation process of vinblastine sulfate (VBLS)-loaded folate-conjugated bovine serum albumin (BSA) nanoparticles for tumor-targeted drug delivery using response surface methodology (RSM). Int J Nanomedicine. 2009;4:321-33. https://doi.org/10.2147/IJN.S8501
54. Bronze-Uhle ES, Costa BC, Ximenes VF, Lisboa-Filho PN. Synthetic nanoparticles of bovine serum albumin with entrapped salicylic acid. Nanotechnol Sci Appl. 2016;10:11-21. https://doi.org/10.2147/NSA.S117018
55. Solanki R, Patel K, Patel S. Bovine Serum Albumin Nanoparticles for the Efficient Delivery of Berberine: Preparation, Characterization and In vitro biological studies. Colloids and Surfaces A: Physicochemical and Engineering Aspects. 2021;608:125501. https://doi.org/10.1016/j.colsurfa.2020.125501
56. Tirkey B, Bhushan B, Uday Kumar S, Gopinath P. Prodrug encapsulated albumin nanoparticles as an alternative approach to manifest anti-proliferative effects of suicide gene therapy. Materials Science and Engineering: C. 2017;73:507-15. https://doi.org/10.1016/j.msec.2016.12.108
57. Rohiwal SS, Satvekar RK, Tiwari AP, Raut AV, Kumbhar SG, Pawar SH. Investigating the influence of effective parameters on molecular characteristics of bovine serum albumin nanoparticles. Applied Surface Science. 2015;334:157-64. https://doi.org/10.1016/j.apsusc.2014.08.170
58. Maheux CR, Alarcon IQ, Copeland CR, Cameron TS, Linden A, Grossert JS. Identification of polymorphism in ethylone hydrochloride: synthesis and characterization. Drug Test Anal. 2016;8(8):847-57. https://doi.org/10.1002/dta.1859

59. Khodashenas B, Ardjmand M, Sharifzadeh Baei M, Shokuhi Rad A, Akbarzadeh Khiyavi A. Bovine serum albumin/gold nanoparticles as a drug delivery system for Curcumin: experimental and computational studies. Journal of Biomolecular Structure and Dynamics. 2020;38(15):4644-54. https://doi.org/10.1080/07391102.2019.1683073
60. Carapina da Silva C, Pacheco BS, das Neves RN, Dié Alves MS, Sena-Lopes Â, Moura S, et al. Antiparasitic activity of synthetic curcumin monocarbonyl analogues against Trichomonas vaginalis. Biomedicine & Pharmacotherapy. 2019;111:367-77. https://doi.org/10.1016/j.biopha.2018.12.058
61. Hasanpoor Z, Mostafaie A, Nikokar I, Hassan ZM. Curcumin-human serum albumin nanoparticles decorated with PDL1 binding peptide for targeting PDL1-expressing breast cancer cells. Int J Biol Macromol. 2020;159:137-53. https://doi.org/10.1016/j.ijbiomac.2020.04.130
62. Huang D, Chen YS, Rupenthal ID. Hyaluronic Acid Coated Albumin Nanoparticles for Targeted Peptide Delivery to the Retina. Mol Pharm. 2017;14(2):533-45. https://doi.org/10.1021/acs.molpharmaceut.6b01029
63. Merodio M, Arnedo A, Renedo MJ, Irache JM. Ganciclovir-loaded albumin nanoparticles: characterization and in vitro release properties. Eur J Pharm Sci. 2001;12(3):251-9. https://doi.org/10.1016/S0928-0987(00)00169-X
64. Sadeghi R, Moosavi-Movahedi AA, Emam-jomeh Z, Kalbasi A, Razavi SH, Karimi M, et al. The effect of different desolvating agents on BSA nanoparticle properties and encapsulation of curcumin. Journal of Nanoparticle Research. 2014;16(9):2565. https://doi.org/10.1007/s11051-014-2565-1
65. Nosrati H, Abbasi R, Charmi J, Rakhshbahar A, Aliakbarzadeh F, Danafar H, et al. Folic acid conjugated bovine serum albumin: An efficient smart and tumor targeted biomacromolecule for inhibition folate receptor positive cancer cells. Int J Biol Macromol. 2018;117:1125-32. https://doi.org/10.1016/j.ijbiomac.2018.06.026
66. Costa P, Sousa Lobo JM. Modeling and comparison of dissolution profiles. Eur J Pharm Sci. 2001;13(2):123-33. https://doi.org/10.1016/S0928-0987(01)00095-1
67. Li NN, Fu CP, Zhang LM. Using casein and oxidized hyaluronic acid to form biocompatible composite hydrogels for controlled drug release. Mater Sci Eng C Mater Biol Appl. 2014;36:287-93. https://doi.org/10.1016/j.msec.2013.12.025
68. Rezaei A, Nasirpour A. Evaluation of Release Kinetics and Mechanisms of Curcumin and Curcumin-β-Cyclodextrin Inclusion Complex Incorporated in Electrospun Almond Gum/PVA Nanofibers in Simulated Saliva and Simulated Gastrointestinal Conditions. BioNanoScience. 2019;9(2):438-45. https://doi.org/10.1007/s12668-019-00620-4
69. Delfiya D, Kulandasamy T. Evaluation of in vitro release pattern of curcumin loaded egg albumin nanoparticles prepared using acetone as desolvation agent. 2016;10:126-35.
70. Maboudi SA, Shojaosadati SA, Aliakbari F, Arpanaei A. Theranostic magnetite cluster@silica@albumin double-shell particles as suitable carriers for water-insoluble drugs and enhanced T2 MR imaging contrast agents. Mater Sci Eng C Mater Biol Appl. 2019;99:1485-92. https://doi.org/10.1016/j.msec.2019.02.063